JMB

Vibrational Dynamics of Transfer RNAs: Comparison of the Free and Synthetase-bound Forms

Ivet Bahar[1,2] and Robert L. Jernigan[1]*

[1]*Molecular Structure Section Laboratory of Experimental and Computational Biology Division of Basic Sciences National Cancer Institute National Institutes of Health Bethesda, MD 20892-5677 USA*

[2]*Chemical Engineering Department & Polymer Research Center, Bogazici University and TUBITAK Advanced Polymeric Materials Research Center, Bebek 80815 Istanbul, Turkey*

The vibrational dynamics of transfer RNAs, both free, and complexed with the cognate synthetase, are analyzed using a model (Gaussian network model) which recently proved to satisfactorily describe the collective motions of folded proteins. The approach is similar to a normal mode analysis, with the major simplification that no residue specificity is taken into consideration, which permits us (i) to cast the problem into an analytical form applicable to biomolecular systems including about 10^3 residues, and (ii) to acquire information on the essential dynamics of such large systems within computational times at least two orders of magnitude shorter than conventional simulations. On a local scale, the fluctuations calculated for yeast tRNA^{Phe} and tRNA^{Asp} in the free state, and for tRNA^{Gln} complexed with glutaminyl-tRNA synthetase (GlnRS) are in good agreement with the corresponding crystallographic *B* factors. On a global scale, a hinge-bending region comprising nucleotides U8 to C12 in the D arm, G20 to G22 in the D loop, and m^{7}G46 to C48 in the variable loop (for tRNA^{Phe}), is identified in the free tRNA, conforming with previous observations. The two regions subject to the largest amplitude anticorrelated fluctuations in the free form, i.e. the anticodon region and the acceptor arm are, at the same time, the regions that experience the most severe suppression in their flexibilities upon binding to synthetase, suggesting that their sampling of the conformational space facilitates their recognition by the synthetase. Likewise, examination of the global mode of motion of GlnRS in the complex indicates that residues 40 to 45, 260 to 270, 306 to 314, 320 to 327 and 478 to 485, all of which cluster near the ATP binding site, form a hinge-bending region controlling the cooperative motion, and thereby the catalytic function, of the enzyme. The distal β-barrel and the tRNA acceptor binding domain, on the other hand, are distinguished by their high mobilities in the global modes of motion, a feature typical of recognition sites, also observed for other proteins. Most of the conserved bases and residues of tRNA and GlnRS are severely constrained in the global motions of the molecules, suggesting their having a role in stabilizing and modulating the global motion.

© 1998 Academic Press

Keywords: tRNA-synthetase complex; vibrational dynamics; recognition and binding; collective motions; *B* factors

*Corresponding author

Introduction

A comprehensible description of the conformational preference of tRNAs on a global scale is essential for understanding the mechanisms of their molecular recognition, translation of the gen-

etic code, and other diverse functions in the cell. Starting with the determination of the crystal structure of tRNA^{Phe} (Robertus *et al.*, 1974; Jack *et al.*, 1976; Sussman *et al.*, 1978; Hingerty *et al.*, 1978), several experimental and theoretical studies aimed at characterizing the types of internal motions intrinsic to the unique L-shaped tertiary structure of tRNAs in the folded state (Rigler & Wintermeyer, 1983; McCammon & Harvey, 1987). Current studies indicate that the three-dimensional L-form of tRNAs is universal, and simple structural rules about the lengths of helical domains and

the number of stacked nucleotides, together with conformational compensations that ensure appropriate tertiary stacking of nucleotides, can rationalize disparate structural features of certain (mitochondrial) tRNAs (Steinberg *et al.*, 1997). The occurrence of common, simple structure-related rather than sequence-specific characteristics of tRNAs is also indicated by a recent study in which the recognition of the T-arm by tRNA (M^{5}U54)-methyltransferase, the enzyme catalyzing the methylation of U54 of tRNAs, is shown to reside in the three-dimensional structure of the seven member T-loop rather than in its primary structure (Gu *et al.*, 1996). These observations suggest that the dynamics of tRNAs should also obey certain general rules, regardless of the specific type of nucleotides or base-pairs, these being imparted by the unique three-dimensional shape of the molecule subject to a network of secondary and tertiary contacts.

Recently, we developed a simple mechanical model for describing the dynamics of proteins near the folded state (Bahar *et al.*, 1997, 1998a,b; Haliloglu *et al.*, 1997; Jernigan & Bahar, 1998). The model takes account of the joint effect of all secondary and tertiary contacts at the residue level. The folded state is assumed to be maintained by a network of uniform potentials between all residue pairs, bonded or non-bonded, located within a certain interaction range. The interaction potentials are assumed to be harmonic such that residues are subject to Gaussianly distributed fluctuations about their mean positions, hence the name Gaussian network model (GNM). A single parameter, γ, is adopted for the force constant of the harmonic potentials, following the original study by Tirion (1996). Application of the GNM to a series of proteins demonstrated its power for describing (i) the detailed fluctuation amplitudes of residues in folded structures (Bahar *et al.*, 1997), in excellent agreement with crystallographic temperature factors, (ii) the vibrational dynamics in the native state in close conformity with detailed normal mode analyses (Haliloglu *et al.*, 1997), and (iii) the hydrogen exchange behavior of individual residues under native state or weakly denaturing conditions (Bahar *et al.*, 1998a).

Here, the GNM will be used for the conformational analysis of tRNAs, both in the free state, and bound to aminoacyl-tRNA synthetase. The tRNA molecule is stabilized by a network of Watson-Crick-type base-pairs, as well as tertiary base-pairs, base-triplets, and other interactions, including the stacking of 71 bases out of 76 in yeast tRNA^{Phe}, for example. Two domains are defined for describing the L-shaped structure, the first formed by the stacking of the anticodon stem onto the D stem, and the second resulting from the coaxial stacking of the TΨC stem onto the acceptor helix. The tight packing of nucleotides *via* unusual base-stacking patterns suggests a high cooperativity between the different structural elements of the molecule, which may be suitably characterized by

the GNM formalism. We will consider crystal structures available in the Protein Data Bank (PDB; Abola *et al.*, 1987; Bernstein *et al.*, 1977). Most of the calculations for the tRNA in the free form will be performed using the crystal structures of yeast tRNA^{Phe} (Jack *et al.*, 1976; Sussman *et al.*, 1978; Westhof & Sundaralingam, 1986; Westhof *et al.*, 1988). These structures, refined up to 2.5 Å resolution, are closely superimposable, despite their being packed in different crystal forms. Similar calculations for tRNA^{Asp} indicated that the dominant structural features are common, with minor sequence-dependent differences, to both yeast tRNAs. For tRNA complexed with aminoacyl-tRNA synthetase, we will consider the crystal structure of tRNA^{Gln} complexed with *Escherichia coli* glutaminyl-tRNA synthetase (GlnRS) and ATP, determined (Rould *et al.*, 1989) and refined at 2.5 Å resolution (Rould *et al.*, 1991) by Steitz and collaborators.

Two fundamental properties are included in the model: (i) the local packing density, which is conveniently expressed in terms of a nucleotide coordination number, or the number of neighbors within the first shell of interaction, and (ii) the topology of non-bonded contacts, which accounts for all interactions stabilizing the folded state, including Watson-Crick base-pairing and all other close interactions. No energy functions or parameters specific to the nucleotide base-pairs are utilized. A simple analytical approach is adopted, which will be verified to yield a satisfactory description of tRNA dynamics upon comparison with (i) crystallographic temperature factors, and (ii) results from simulations which require two orders of magnitude longer computation times. A description of the model and method is presented in Materials and Methods. Basically, conformational preferences are determined by an eigenvalue analysis of the so-called Kirchhoff matrix of contacts, Γ, characteristic of the structure investigated. The utility of such eigenvalue analyses has been demonstrated in other studies. Here, we decompose the vibrational motions into a collection of modes, similar to a normal mode analysis, and subsequently focus on the slowest modes which, in principle, reflect the motions most related to function (Bahar *et al.*, 1998b) occurring on the most global scale.

In the large amplitude elastic motions of tRNA elucidated by focusing on the slow-modes regime, the anticodon trinucleotide and amino acid acceptor stem will be shown to undergo highly concerted but opposite direction (anticorrelated) fluctuations, when the molecule is uncomplexed. A group of nucleotides, mostly located in the D-arm, will be distinguished by their unique dynamic characteristics, which will be attributed to their involvement in modulating the hinge-bending motion of the molecule. In the form bound to GlnRS, on the other hand, a drastic change in the vibrational dynamics of the tRNA will be observed compared to that of the uncomplexed tRNA. The

fact that the equilibrium structure of the enzyme-bound tRNA differs from the known structures of uncomplexed tRNA molecules, especially at the anticodon loop, was pointed out by Steitz and collaborators (Rould *et al.*, 1991). Here, we will show that the vibrational dynamics of the enzyme-bound tRNA, in addition to its equilibrium structure, differs extensively from that of the uncomplexed tRNAs. The tRNA^{Gln} nucleotides and GlnRS residues most strongly affected by complex formation will be identified, and their role in recognition and global motion will be discussed.

Results and Discussion

Fluctuations of nucleotides in tRNA crystals: comparison with crystallographic *B* factors

Figure 1 displays the mean-square (m.s.) fluctuations in the positions of tRNA nucleotides expressed in terms of the crystallographic *B* factors $B_i = 8\pi^2 \langle \Delta \mathbf{R}_i \cdot \Delta \mathbf{R}_i \rangle / 3$. Here $\Delta \mathbf{R}_i$ refers to the change in the position vector $\mathbf{R}_i$ of the *i*th nucleotide, with respect to its mean (crystal) coordinates. Figure 1(a) and (b) displays the results obtained for yeast tRNA^{Phe} (monoclinic; Westhof & Sundaralingam, 1986) and yeast tRNA^{Asp} (form B); Westhof *et al.*, 1988), respectively. Theoretical (GNM) results are shown by the continuous curves, and measurements from X-ray crystallogra-
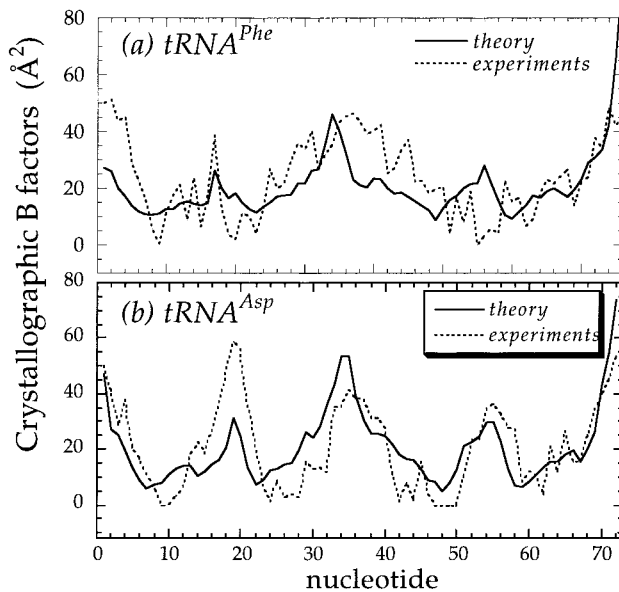
Figure 1. Comparison of crystallographic temperature factors (broken curves) $B_i = 8\pi^2 \langle \Delta \mathbf{R}_i \cdot \Delta \mathbf{R}_i \rangle / 3$ and results calculated from GNM (continuous curves), for (a) yeast tRNA^{Phe} and (b) yeast tRNA^{Asp}. Mean-square fluctuations $\langle \Delta \mathbf{R}_i \cdot \Delta \mathbf{R}_i \rangle$ are calculated using equation (2). The Kirchhoff matrix Γ therein is constructed on the basis of the phosphorus atoms' coordinates reported in the PDB structures 1TRA (Westhof & Sundaralingam, 1986) and 2TRA (Westhof *et al.*, 1988), respectively. Experimental curves refer to the temperature factors of the Phosphorus atoms in the structures.

phy (Westhof & Sundaralingam, 1986; Westhof *et al.*, 1988) by the dotted curves. GNM calculations repeated using the coordinates of yeast tRNA^{Phe} crystallized in orthorhombic form (Westhof *et al.*, 1988) yielded a fluctuation distribution curve (not shown) very similar to that in Figure 1(a).

Theoretical $\langle \Delta \mathbf{R}_i \cdot \Delta \mathbf{R}_i \rangle$ values are found from the diagonal elements $[\Gamma^{-1}]_{ii}$ of the inverse Kirchhoff matrices constructed for tRNA^{Phe} and tRNA^{Asp} using the phosphorus atom coordinates of the respective PDB files 1TRA and 2TRA (see equation (3) in Materials and Methods). A harmonic potential force constant (γ) given by $3kT/\gamma = 12$ Å^2 is used for all contacting nucleotides, which follows from the normalization of the theoretical curves with respect to the experimental ones. The number of contacts z_i that a given nucleotide *i* makes with the neighbors is the basic ingredient for constructing Γ. The diagonal elements of Γ are identically equal to z_i. Consequently, $\langle \Delta \mathbf{R}_i \cdot \Delta \mathbf{R}_i \rangle$ scales with $1/z_i$, as a first order approximation when Γ^{-1} is replaced by a series expansion about the diagonal matrix formed by the elements $1/z_i$, $1 \leqslant i \leqslant n$. Comparison of theoretical curves with properly rescaled inverse contact numbers, showed indeed that the m.s. fluctuations are closely determined by the reciprocals of contact numbers. The cutoff separation r_c adopted for defining the distance range of contacts between nucleotides is an important parameter. Here we used $r_c = 19$ Å, a distance sufficiently large to include all base-pairs and triplets. See Materials and Methods for more details.

We have performed calculations with and without the magnesium ions reported in the PDB structures. A single interaction site per Mg ion was adopted, and the hydration shell was not explicitly considered, in conformity with the level of detail adopted in the GNM approach. No significant changes were observed in the results. This might be understandable in view of the fact that a total of about 1500 contacts (on the basis of 20 contacts, approximately, for each of the 76 nucleotides) are simultaneously considered in the model, and the overall effect of the additional ~60 contacts contributed by the four magnesium ions is relatively weak. The perturbations due to the Mg ions may be summarized as a small decrease in the flexibility of domain 1, together with a slight enhancement in the mobility of the T-loop nucleotides, around T54 and Ψ55.

The agreement between calculated m.s. fluctuations and those indicated by X-ray crystallography is remarkable in view of (i) the simplicity of the theory, and (ii) the possible interferences of crystal packing disorder and/or intermolecular effects that could lead to differences between calculated and measured values (Frauenfelder *et al.*, 1979). Previous calculations of fluctuation amplitudes, using normal mode analysis (Nakamura & Doi, 1994), or molecular dynamics simulations (Harvey *et al.*, 1985; Prabhakaran *et al.*, 1985), do not yield appreciably better agreement with experiment, despite the use of more detailed energy

functions and parameters, and complex energy minimization and simulation algorithms.

The fluctuations presently found with the GNM bear a close resemblance to those obtained in previous detailed computations. For example, Gm34 of tRNA^{Phe} is distinguished in all theoretical curves by a sharp peak, in contrast to the experimental curve, which is relatively flat near the anticodon region. This difference may result from crystal packing effects. In the crystal, nucleotide 34 is stacked onto nucleotide 34 of the symmetry-related molecule. Such intermolecular effects have not been considered here. Likewise, the calculated fluctuations near the TΨC loop exhibit some departure from those indicated by the *B* factors. The amplitude of the motion of D17 in the D-loop is underestimated in both molecular dynamics simulations (Prabhakaran *et al.*, 1985), and the present calculations; whereas it is more accurately captured by Nakamura & Doi (1994). The m.s. fluctuations obtained here for tRNA^{Asp}, on the other hand, exhibit a better agreement with the experimental data, than that (Nakamura & Doi, 1994) previously found. Overall, the comparison presented in Figure 1 is supportive of the use of the GNM as an effective first order approach for investigating the dynamics of tRNAs.

Global motion in free tRNA: relative flexibilities of nucleotides

Figure 2 displays the regions with differing extents of flexibility identified by the GNM approach for tRNA^{Phe}. Nucleotides are colored in blue, green, yellow, orange and red, in order of decreasing mobilities in the global mode of motion of the molecule. For clarity, results are presented in two different forms: (a) clover leaf secondary structure representation of the tRNA^{Phe} sequence, and (b) a three-dimensional ribbon diagram.

The categories shown by different colors are chosen with reference to the distribution of m.s. fluctuations displayed in Figure 3. In this Figure $\langle \Delta \mathbf{R}_i \cdot \Delta \mathbf{R}_i \rangle_k$ values for the largest amplitude/slowest ($k = 2$) mode of motion are displayed, as a function of nucleotide index. The distribution curves are normalized, i.e. the total enclosed areas are equal to unity. The horizontal lines are drawn to separate nucleotides of different flexibilities.

Nucleotides in the uppermost part are the most mobile in the global motion of the molecule. These are shown in blue in Figure 2. These comprise the anticodon trinucleotide G$_m$AA, together with four neighboring nucleotides in the anticodon loop, and the ACCA tetranucleotide at the acceptor end. We note that the N73 "discriminator" base, which is critically important for aminoacylation specificity and efficiency (Schimmel & dePoupiana, 1995), is among the group of most mobile nucleotides in the free form of tRNA, together with the other functionally important nucleotides. This group is succeeded by one of intermediate flexibility (green),

including the adjoining nucleotides, in both the acceptor helix and the anticodon arm. Next, a region of relatively low flexibility is identified, shown in yellow. This region includes four discontinuous stretches of nucleotides along the sequence, although these all cluster together into two regions (domain centers) in the folded conformation.

Finally, the lowermost portion in Figure 3 corresponds to nucleotides subject to highly restrictive motions. This region is enlarged in the inset, and further divided into two subsets by the horizontal line. The nucleotides above the line are shown in orange in Figure 2, and those below, in red. Nucleotides in the latter subset are practically frozen. This suggests that they are located on or near the hinge bending axis, which is fixed in space, during the collective motion. They should in principle play a critically important role in controlling the overall function of the molecule. These are bases 8 to 15 and 20 to 22 in the D-stem, 46 to 48 in the variable loop, and 59 in the TΨC-loop. Those in the D-stem and in the variable loop are confirmed below to be located on the hinge-bending axis. U59 is the only nucleotide located farther away from the hinge-bending region. We note, however, that nucleotide 59 was recently proposed to be an important element, its stacking against domain 1 being essential for the integrity of the overall L-shaped structure of tRNAs (Steinberg *et al.*, 1997).

A striking observation is that all of the conserved nucleotides, except for the CCA sequence at the 3'-OH terminus, and U33 at the anticodon loop, are at the lowermost portion of the fluctuation distribution curve displayed in Figure 3. These are shown by the filled circles along the curve. In other words, all of the conserved nucleotides participate in the most rigid structural element of the molecule with respect to its global motion. This supports the view that the conservation of these nucleotides is linked to the conservation of the global motions of tRNA.

Orientational correlations between nucleotide motions

The degree of orientational correlation between nucleotide motions is found from equations (4) or (5) presented in Materials and Methods. Here, the off-diagonal terms of the Γ^{-1} matrix (or its *k*th mode counterpart) are normalized with respect to the diagonal elements, such that the effects of the amplitudes of motions are eliminated, and pure orientational correlations, are extracted.

Orientational correlations C_{ij} vary in the range $-1 \leqslant C_{ij} \leqslant 1$, in general; the lower and upper limits refer to fully anticorrelated and correlated motions, respectively, with $C_{ij} = 0$ for uncorrelated motions. In multivariate processes, such as the conformational dynamics of tRNA, preferences are obscured due to the superposition of multiple modes, and the orientational correlations appear to

be relatively weak. Examination of isolated modes, on the other hand, gives a clearer picture: the values $C_{ij} = \pm 1$ or 0, are assigned, exclusively, to each nucleotide pair in a single mode k. Thus, nucleotides i and j move either in the same direction $(+1)$, or in the opposite direction (-1) along the kth mode coordinate, unless one or the other is stationary (0) or has no component along this coordinate axis.

The results obtained for the slowest mode of tRNA^{Phe} are presented in Figure 4. This is the correlation map C_{ij} evaluated using equation (5) in Materials and Methods for the slowest (global) mode of motion $(k = 2)$. The two axes represent the nucleotide sequence numbers i and j. The red regions refer to the pairs exhibiting a positive correlation $(C_{ij} = 1)$, while the regions shown in blue describe those undergoing opposite sense motions
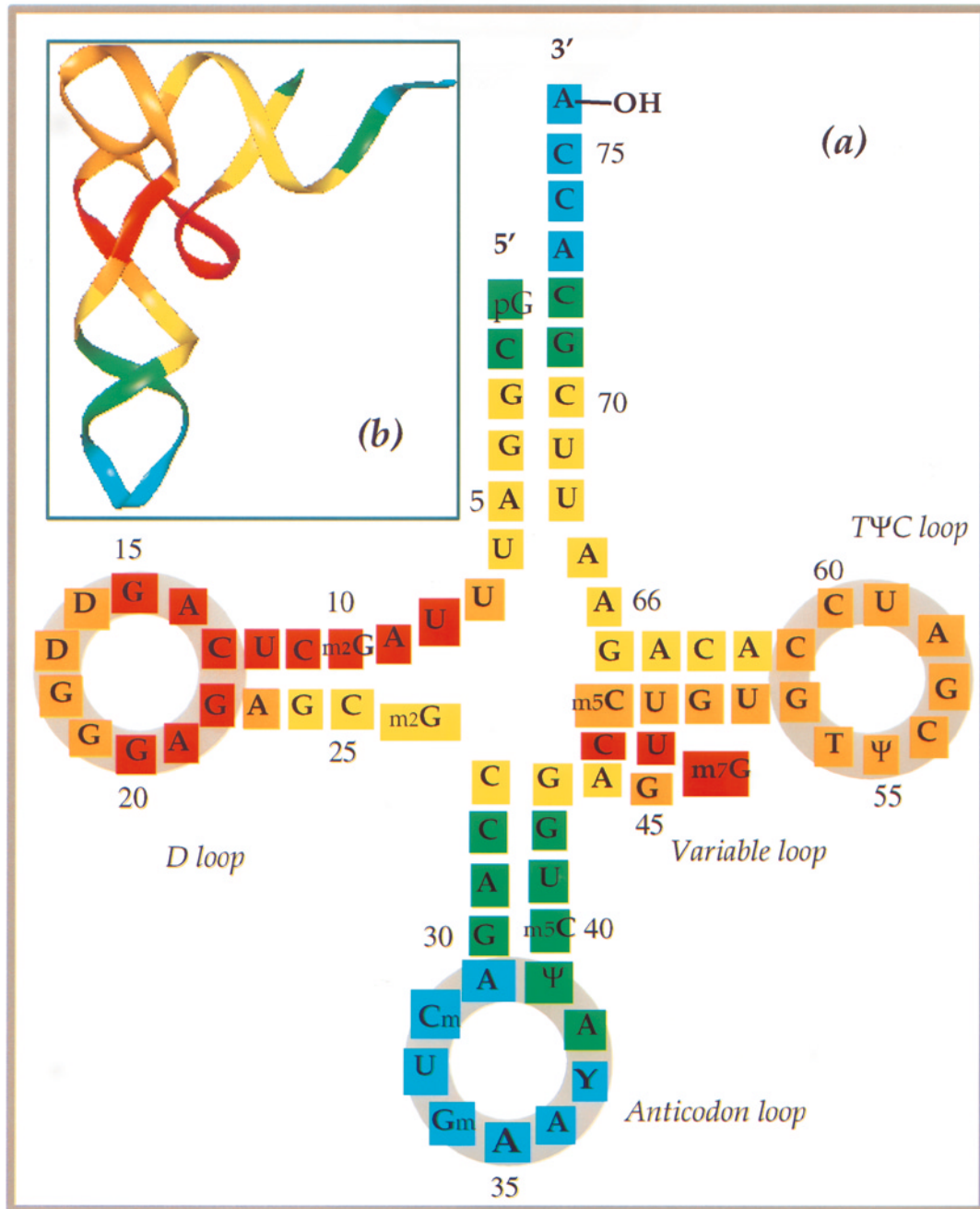
Figure 2. Nucleotide regions with various extents of flexibility in tRNA^{Phe}, shown in red, orange, yellow, green and blue, in order of increasing mobility in the global conformational motion, presented in (a) clover-leaf representation, and (b) ribbon diagram. The nucleotides shown in red, are almost rigid in the slowest (global) mode of motion of folded tRNA^{Phe}, and therefore may be viewed as forming the hinge region of the molecule. At the other extreme, nucleotides exhibiting the largest amplitude motions, shown in blue, we observe those in the anticodon loop and the CCA sequence at the amino acid acceptor end. Note that base 59 should be red and 62 should be orange.
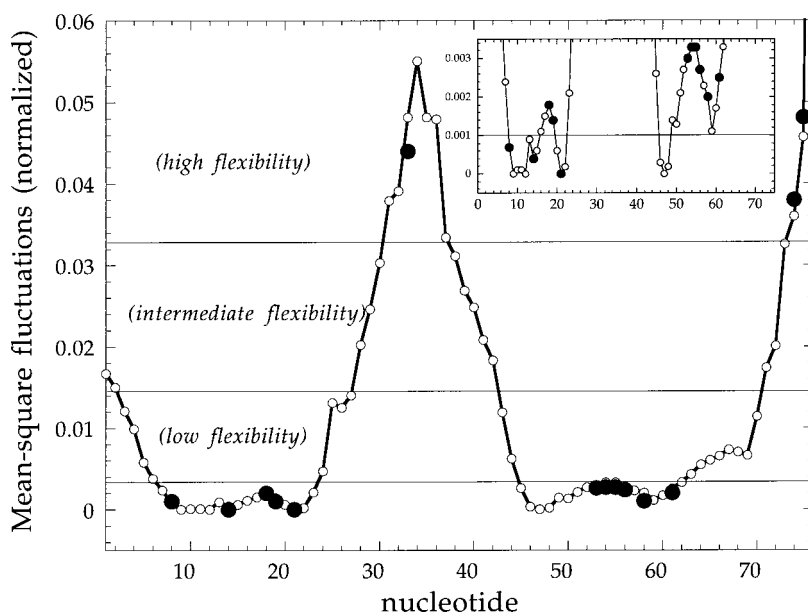
Figure 3. Mean-square fluctuations $\langle \Delta \mathbf{R}_i \cdot \Delta \mathbf{R}_i \rangle_k$ of tRNA^{Phe} nucleotides in the global mode of motion ($k = 2$). Results are normalized, i.e. the area under the curve is unity. Minima refer to severely restricted or rigid regions; whereas maxima are the most flexible regions. Horizontal lines divide the structure into regions of different flexibilities. Nucleotides in the uppermost (high flexibility) region are colored blue in Figure 2. The intermediate and low flexibility regions are the green and yellow nucleotides. The lowermost portion, which includes most of the constant nucleotides (shown in filled circles), is enlarged in the inset. This region is further divided into two groups of nucleotides, shown in orange and red in Figure 2.

($C_{ij} = -1$). The white regions refer to residues which do not exhibit a correlation ($C_{ij} = 0$). Instead, they undergo no motion, or motions normal to the dominant direction defined by the slowest mode.

The most striking feature in the correlation map displayed in Figure 4 is the occurrence of long stretches of nucleotides, behaving as rigid blocks;
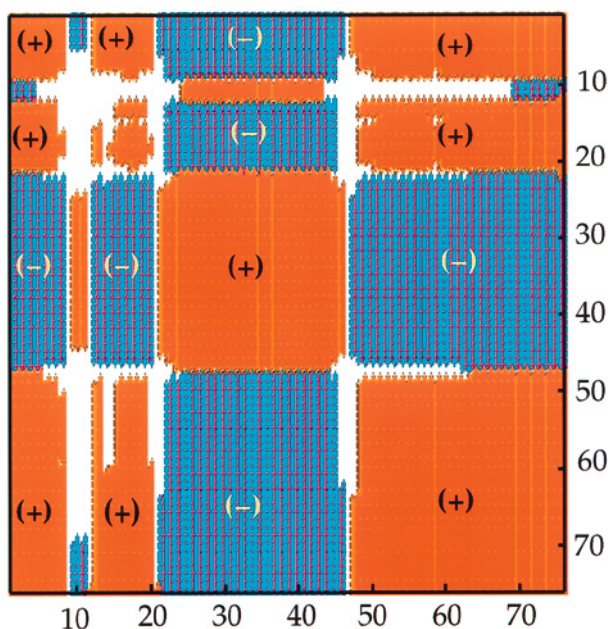
Figure 4. Correlation map for nucleotide motions in the global conformational mode of tRNA^{Phe}. The regions colored red describe the nucleotide pairs undergoing motions in the same direction ($C_{ij} = 1$); blue regions refer to those subject to opposite direction displacements ($C_{ij} = -1$), and uncolored regions refer to uncorrelated pairs ($C_{ij} = 0$). Nucleotides in the last group are either stationary, or move along a direction normal to that of the global mode of motion. These are shown in yellow in Figure 5.

for example, nucleotides 49 to 76 in the second domain form a concerted block. Their direction of motion is identical to that of nucleotides 1 to 19 in the same domain, except for a few nucleotides exhibiting uncorrelated (U8, A9 and U12), or anti-correlated (m^{2}G10 and C11) motions. We note that these regions cover the entire TΨC arm, the amino acid acceptor stem, and the D loop. On the other hand, nucleotides 23 to 45 form another block moving in the opposite direction to the first. Nucleotides m^{2}G10 and C11 are coupled to this block to some extent. This second block includes the entire anticodon arm and part of the variable loop, as well as some portions of the D arm, excluding the D loop. These two blocks are displayed in red and blue, respectively, in Figure 5, where the structure is shown from two different perspectives, together with its ribbon representation. In the side view on the right, the nucleotides D16 to G18 of the D loop and U47 of the variable arm protrude to the right and left, respectively, of the plane defined by the L-shape.

The nucleotides lying outside these blocks exhibit a more complex behavior. They are either totally stationary (A9, U12, A21, U47) or occasionally coupled to one or the other block (U8, m^{2}G10, C11, G20, G22, m^{7}G46, C48). Interestingly, these (shown in yellow in Figure 5) are all located in the most rigid region identified in the previous section (see the section colored in red in Figure 2). The involvement of these residues in the hinge bending mechanism of the overall molecule is thus evidenced both by their restricted mobility demonstrated above, and by their lack of preferred orientation in the slowest mode revealed here.

In the early study of the 3.0 Å resolution crystal structure of tRNA^{Phe}, Robertus *et al.* (1974) suggested a hinge between the D stem and the anticodon stem, which correlates with the region presently identified. Olson *et al.* (1976) proposed a
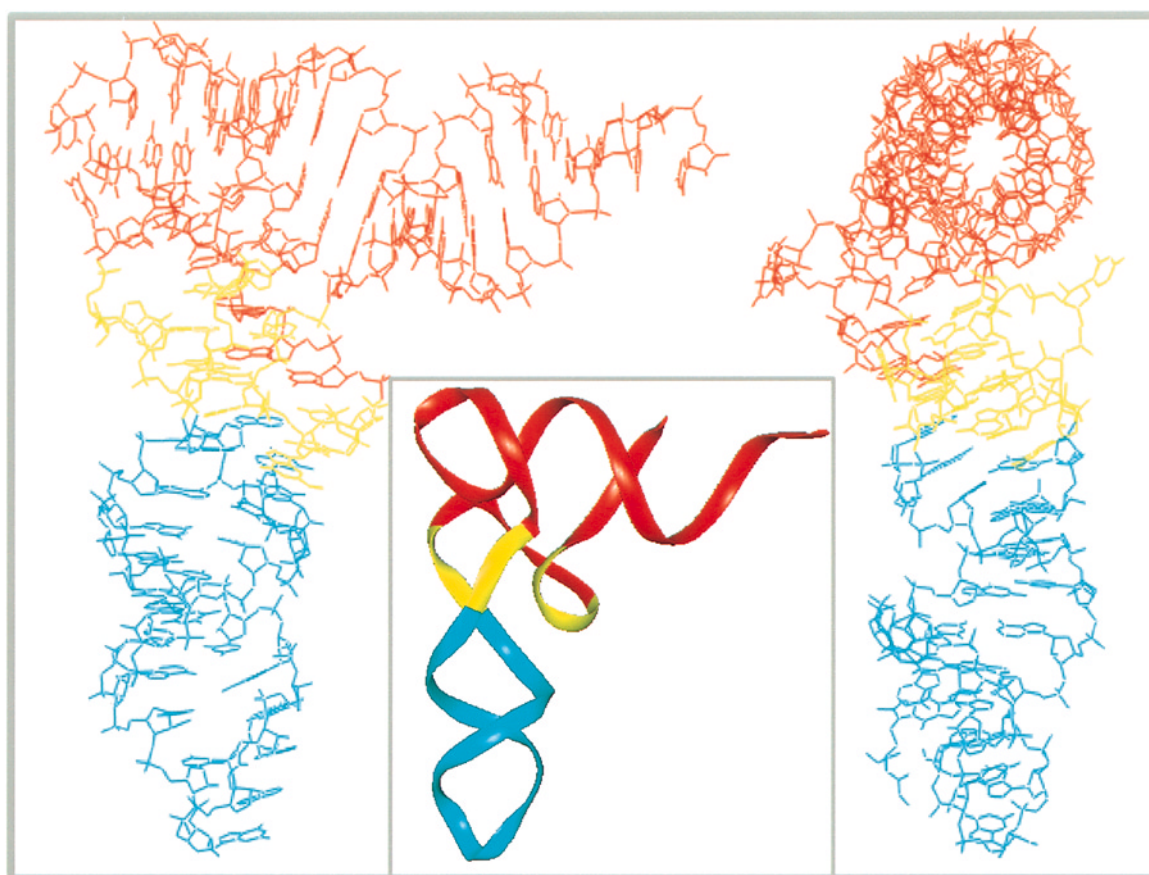
Figure 5. Schematic representation of structural units, or blocks, exhibiting coherent motions in the slowest mode of motion of tRNA[Phe], shown in three different forms. The nucleotides colored in red all exhibit the same direction of motion in the slowest mode, while those colored in blue also move coherently, but in the opposite direction with respect to the first block. These regions are identified from the correlation map in Figure 4. Nucleotides shown in yellow are U8 to U12, G20 to G22, and m[7]G46 to C48. The former eight are in the D arm, and the latter three in the variable loop (see Figure 1(a)). These nucleotides are proposed to form the hinge region of the molecule.

hinge near the elbow of the L-shape, containing nucleotides U8, A9, m[7]G46, U47 and C48, based on their laser light scattering measurements. These overlap with the region presently identified. Tung *et al*. (1984) calculated the energy costs of deforming the tRNA with respect to different hinge regions using an adiabatic mapping method (McCammon & Harvey, 1987), and observed that the bending with respect to a hinge at the phosphates P8 and P49 costs less energy than at other sites. The large scale motions of tRNA[Phe] were also examined by modified molecular dynamics simulations (Harvey & Gabb, 1993), which permitted the observation of a change in bend angle between the two arms of the molecule, from $140°$ in the fully open case, to $37°$, in the closed form. In a normal mode analysis (Nakamura & Doi, 1994) the hinge-bending axis of the first mode was shown to lie between U8 and C48, and for the second mode between U8 and G18.

Calculations performed for the four slowest modes $(2 \leqslant k \leqslant 5)$ yield the correlation maps shown in Figure 6. For clarity, nucleotide pairs showing negative and positive orientational correlations are shown separately in Figure 6(a) and (b).

The innermost regions, indicated by an x, describe the pairs exhibiting the strongest couplings, positive or negative. The maps are symmetric with respect to the diagonal shown in Figure 6(a). We note that the regions identified in Figure 4 to exhibit correlated $(+)$ or anticorrelated $(-)$ motions are preserved here, although the correlations exhibit more diversity. Because results are incorporated for four modes, the contour levels now indicate correlations of various strengths; whereas in Figure 4 only three levels, -1, 0, and 1, are shown.

Vibrational dynamics of tRNA[Gln] complexed with GlnRS

The X-ray crystallographic *B* factors calculated (GNM) and experimentally measured (Rould *et al.*, 1991) for tRNA[Gln] bound to GlnRS are presented in Figure 7. An excellent agreement between theory and experiments is observed, confirming the physical relevance and usefulness of the present approach.

The significant departure of the vibrational dynamics of complexed tRNA from that observed in the free form (see Figure 1) deserves special
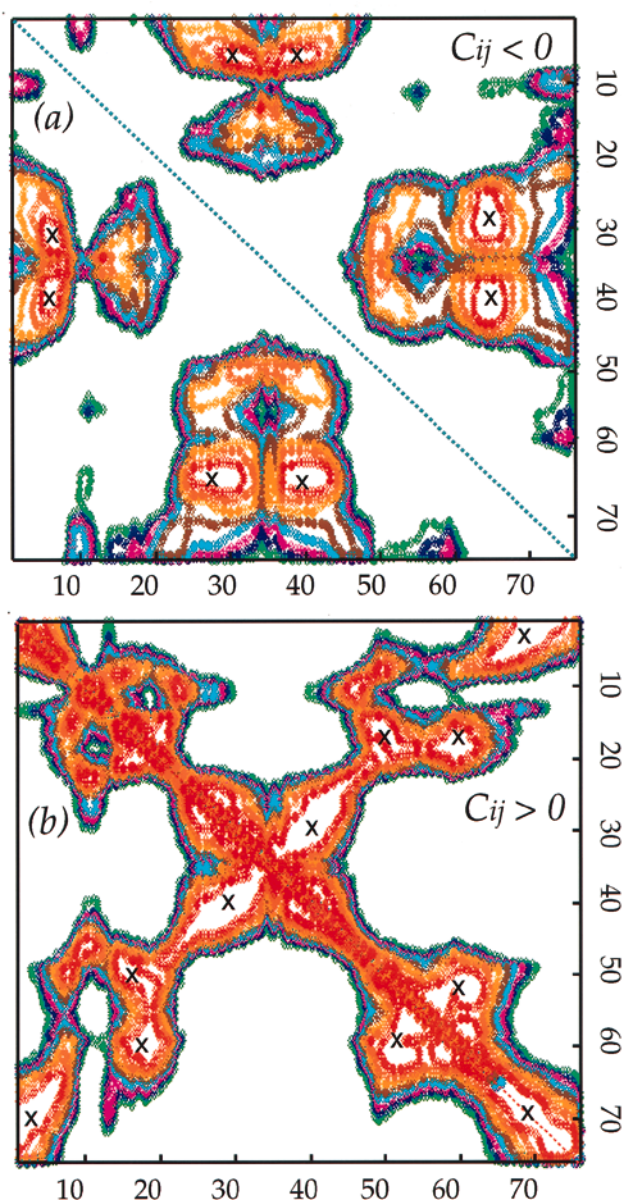
Figure 6. Orientational correlations between nucleotide motions due to the dominant modes of motion $2 \leqslant k \leqslant 5$ of tRNA^{Phe}, calculated using equation (5). The pairs exhibiting negative $(-1 \leqslant C_{ij} \leqslant 0)$ and positive $(0 \leqslant C_{ij} \leqslant 1)$ correlations are displayed separately in maps (a) and (b). The innermost regions enclosed by the red/brown contours and indicated by the x refer to centers of strongest $(|C_{ij}| > 0.88)$ correlation, while the regions outside the green contours, left blank, exhibit the weakest $(|C_{ij}| < 0.24)$ correlation. Seven equally spaced contours are drawn between these two limiting cases.

Figure 7. Comparison of the theoretical and experimental crystallographic *B* factors for tRNA^{Gln} bound to GlnRS. The open circles (and thin curve) refer to experimental data (Rould *et al.*, 1991), and the filled circles (and thick curve) are the results from GNM calculations.

attention. This difference is not due to the distortion in the equilibrium position of the nucleotides in the enzyme-bound form (as we verified by repeating the calculations for the isolated tRNA^{Gln} molecule of the same complex which closely reproduced the curves displayed in Figure 1) but rather to the differences in local packing density experienced by those regions bound to the enzyme. In particular, a severe suppression of the mobility in the anticodon loop is observed, consistent with its interaction with GlnRS. The peak in the fluctuation amplitude curve at this region prior to binding (Figure 1) is now replaced by a minimum, surrounded by two regions of enhanced mobility on the anticodon stem near the loop. The second region experiencing the most important suppression in fluctuation is the −CCA terminus. This end is reported to plunge deeply into a protein pocket (Rould *et al.*, 1989, 1991), which also explains its significant restriction in fluctuations.

The analysis of the vibrational dynamics of the enzyme-bound form of tRNAs requires the simultaneous consideration of the coordinates of both the tRNA and the enzyme interaction sites in the complexed structure. Such a system of about 6000 heavy atoms cannot be accurately characterized by conventional molecular dynamics simulations using present-day computational facilities, due to the excessive time requirement for a complete sampling of the conformational space. In the present analysis, the problem was reduced to the inversion of a matrix, the Kirchhoff matrix of contacts, Γ, characteristic of the complex, of order $2n + m$, where *n* and *m* are the numbers of nucleotides and amino acids in the two respective molecules (see Materials and Methods). And this coarse-grained description, which requires no more than ten minutes CPU time for obtaining the vibrational spectrum (frequencies and mode shapes), serves to reproduce entirely the experimental data.

A more detailed understanding of the collective dynamics of the enzyme-bound tRNA^{Gln} is possible by examining the fluctuations driven by the different modes of motion, and focusing on the slowest modes. The normalized m.s. fluctuations $\langle \Delta \mathbf{R}_i \cdot \Delta \mathbf{R}_i \rangle_k$ contributed by the largest amplitude/
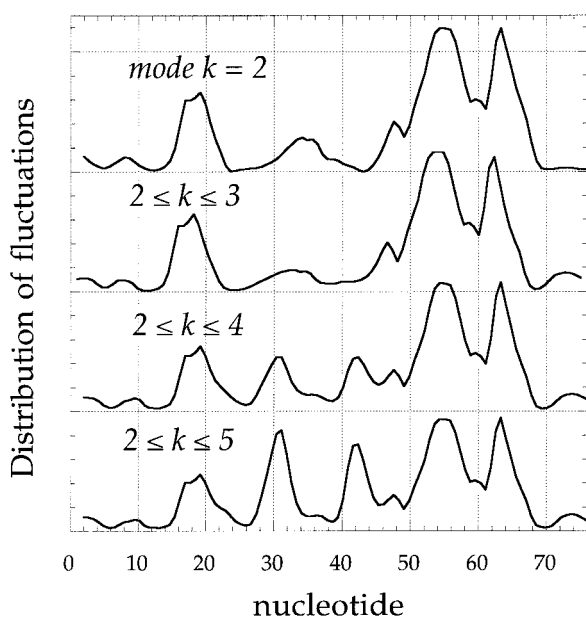
Figure 8. Mean-square fluctuations $\langle \Delta \mathbf{R}_i \cdot \Delta \mathbf{R}_i \rangle_k$ of tRNA^{Gln} nucleotides in the global modes of motion of the complex formed by the tRNA and its synthetase. The uppermost curve describes the motions driven by the slowest/largest amplitude mode; the second, third, and fourth curves display the fluctuations induced by the dominant two, three and four modes, respectively. The four slowest modes already reflect the m.s. fluctuation behavior shown in Figure 7, confirming the dominant role of a few slow modes in controlling the overall dynamics.

slowest mode ($k = 2$), and subsets of modes up to the four slowest ($2 \leqslant k \leqslant 5$), are displayed in Figure 8. The uppermost curve is for the slowest mode of tRNA in the complex. This may be compared with its counterpart in the free form, displayed in Figure 3. A significantly different behavior is observed in the complexed state, although the anticodon region may still be discerned to possess some flexibility in the global motion. The most flexible nucleotides are located, however, in the D-loop (nucleotides 14 to 21), the TΨC loop (53 to 57), and towards the outer elbow portion of the acceptor stem (62 to 66), while nucleotides at conserved positions exhibit relatively restricted motions. No significant change in the distribution of motions is distinguished as we proceed to examine the effect of the two slowest modes ($2 \leqslant k \leqslant 3$). However, starting from the third mode, the distribution changes and rapidly approaches the behavior reflected in the B factors (Figure 7), confirming the dominant role of only a few slow modes in controlling the overall dynamics.

Vibrational dynamics of GlnRS complexed with tRNA^{Gln}

The fluctuation behavior of the bound synthetase induced by the slowest modes of motion is illus-

trated in Figure 9. The uppermost part shows that the distal β-barrel domain of GlnRS (residues 348 to 464), exhibits a high flexibility in the global motion. This region is shown in green in the ribbon diagram of Figure 10. Several of the enzyme's residues which closely interact with the anticodon loop of tRNA are located in this region. Examples of intermolecular interactions involving close (<4.1 Å) interatomic contacts are Val455–C34, Asn413–C34, Gln399–G36, K401–G36, Val455–U35. This suggests that the slowest mode of motion of GlnRS, which ensures a sufficiently large scale movement in space, is related to the recognition of the tRNA anticodon loop. The regions exhibiting the largest amplitude motion in the slowest (global) mode are relevant to recognition or binding of substrates, and this confirms our previous observations (Bahar *et al.*, 1998b; unpublished). Another relatively mobile region in the global motion is the neighboring proximal β-barrel including the C terminus of the chain, which also interferes in the recognition of the anticodon loop. The remainder of the molecule is essentially frozen in this mode.

Examination of the slowest two modes, on the other hand, offers a broader perspective of the con-
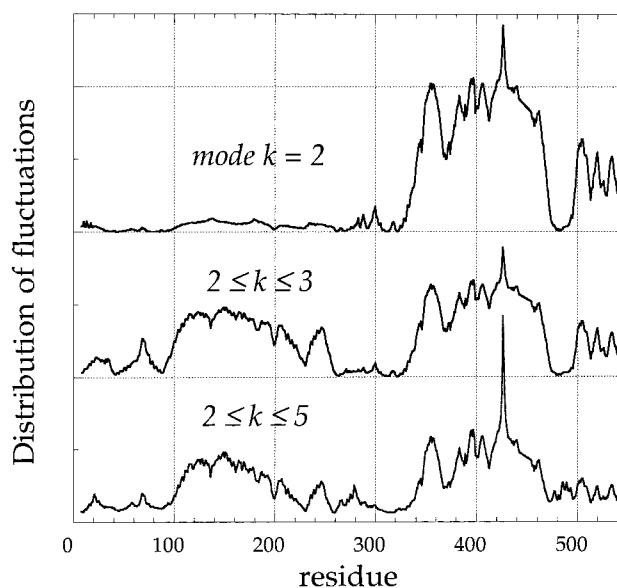
Figure 9. Global modes of motion of GlnRS complexed with tRNA^{Gln}. The m.s. fluctuations of GlnRS residues corresponding to the slowest ($k = 2$) and subsets of the slowest ($2 \leqslant k \leqslant 3$ and $2 \leqslant k \leqslant 5$) modes are shown. In the case of $k = 2$, all the molecule is practically frozen, except for the residues 348 to 464, which form the distal β-barrel (the region colored in green in Figure 10). In the curve labeled $2 \leqslant k \leqslant 3$, another broad peak emerges, at residues 100 to 220 and 235 to 250, which coincide with the acceptor recognition region (shown in yellow in Figure 10). Deepest minima refer to the most severely constrained region (composed of five discontinuous stretches of residues; 40 to 45, 260 to 270, 306 to 314, 320 to 327 and 478 to 485) shown in red in Figure 10.
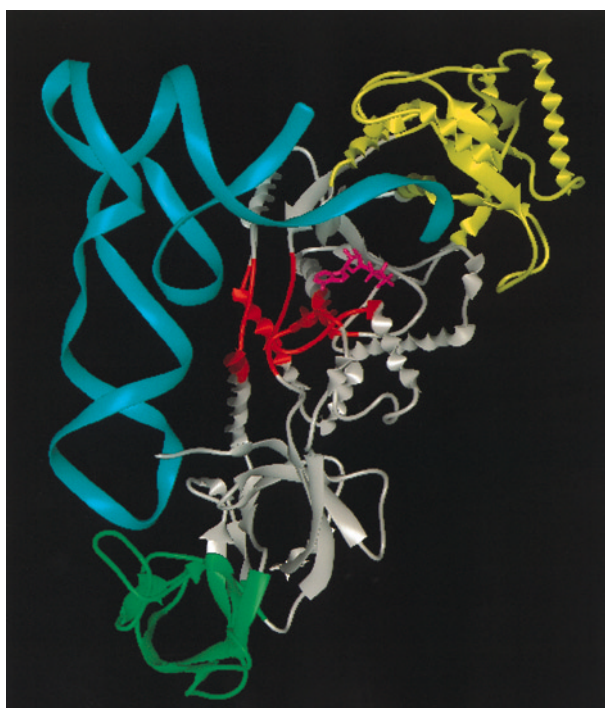
Figure 10. tRNA recognition sites (distal β-barrel, green; and acceptor binding region, yellow) and hinge-bending region (red) of GlnRS revealed by the slowest mode shapes displayed in Figure 9 (see legend to Figure 9). The region shown in red acts as a hinge in monitoring the collective motion (relevant to catalytic function) of the synthetase. The ATP bound in the active site cleft is shown in magenta.

strained (minima) and flexible (maxima) regions of the whole molecule during its collective motion (see the middle curve in Figure 9). As pointed out previously, minima in the slow modes correspond to the hinge-bending regions, during the global motion, as their displacements are negligibly small while the other regions undergo collective fluctuations. In the two dominant ($2 \leqslant k \leqslant 3$) slow modes, minima are observed at various locations along the sequence. A closer examination reveals however that these sequentially distant loci are all clustered at a highly restricted region of the three-dimensional structure, mainly within the Rossmann fold region, which is implicated in the catalytic activity of GlnRS. This region was pointed out by Steitz and co-workers to possess a part ''perhaps most pivotal to the functioning of this enzyme'' (Rould *et al.*, 1989).

Precisely, from the detailed quantitative examination of the m.s. fluctuations driven by the dominant two modes (curve labeled $2 \leqslant k \leqslant 3$ in Figure 9), we identify residues 40 to 45, 260 to 270, 306 to 314, 320 to 327 and 478 to 485 forming the deepest minima. These are shown in red in Figure 10. These are implied by the present GNM analysis to play an essential role in controlling the cooperative motion of the enzyme, and are thereby critically important for catalytic function. Interest-

ingly, this region comprises the two conserved motifs His-Ile-Gly-His (residues 40 to 43) and Met-Ser-Lys (268 to 270) common to the class I aminoacyl-RS, which are located in the active site cleft including the ATP binding site. The cooperative interaction of residues His40 to Ala44, Arg260, Leu261, and Met268 to Lys270 near ATP, was described to be essential for glutaminylation (Perona *et al.*, 1993).

We also observe in the same distribution curve a new broad peak covering residues 100 to 220 and also at 235 to 250. These, shown in yellow in Figure 10, are located in the tRNA acceptor binding domain of the enzyme, another recognition site of the molecule reflected in the broad peaks of the distribution curves in this frequency regime.

The distribution of collective motions is not significantly altered by the contributions of the third and fourth dominant modes, as illustrated in the lower curve of Figure 9. Evidently, the global preferences become gradually less pronounced as the superposition of larger numbers of modes are examined; the most useful information insofar as the global conformational characteristics of the system relevant to function is gathered by extracting the slowest modes.

Conclusion

Here, we have investigated the conformational dynamics of tRNA, both in the free and complexed forms, using a simple model, GNM (Bahar *et al.*, 1997, 1998b; Haliloglu *et al.*, 1997). The comparison of the calculated results with crystallographic *B* factors and other experimental observations, as well as with the results from other more detailed theoretical approaches, demonstrates the utility of the GNM for acquiring rapid, but valuable, information on the conformational dynamics of tRNAs, both on a local and on a global scale. The computational time requirement for this method is at least two orders of magnitude smaller than other methods used to date.

We believe that the success of the model resides in the fact that the cooperativity between all nucleotides and residues is rigorously treated in the model: for example, in the complexed structure, the intricate coupling between the 76 nucleotides and 547 amino acids under the restrictions imposed by all secondary and tertiary contacts, both intramolecular and intermolecular, is simultaneously taken into account by the inversion of the Kirchhoff matrix characteristic of the complex. Insights into the intrinsic dynamic preferences of both the tRNA and its cognate synthetase are obtained, specially through focus upon the slowest, most cooperative modes of motion controlling the global movements relevant to function.

For a quantitative correspondence between theoretical m.s. fluctuations and experimental temperature factors, we adopted here a force constant of $\gamma \approx 0.15$ kcal/(mol Å^2) at $T = 300$ K. On the

other hand, our previous examination of vibrational mode spectra for a series of proteins indicated that, in the folded state, the ratio of the effective friction coefficient (ξ) to force constant is approximately $\xi / \gamma = 6$ ps (Haliloglu *et al.*, 1997), which leads to an effective diffusivity of $kT / \xi = 6.5 \times 10^{-7}$ cm^2/s = 6.5 Å^2/ns. The relatively large fluctuations' m.s. amplitudes are about 60 Å^2 (Figures 1 and 7), which, combined with the above data, indicate a time scale of the order of tens of nanoseconds for the concerted (hinge-bending) vibrational motions. Characterization of these processes on a computer, requires about ten times longer (∼100 ns) MD simulations, which is prohibitively time-consuming with current computational resources.

Dynamic characteristics of tRNAs in the free state

The agreement between the calculated m.s. fluctuations and crystallographic *B* factors (Westhof & Sundaralingam, 1986; Westhof *et al.*, 1988) was satisfactory given the simplicity and efficiency of the method. Nucleotides participating in the hinge-bending region were located as U8 to U12 and G20 to G22 at the D stem, and m^{7}G46 to C48 in the variable loop, in close agreement with those identified by light scattering measurements (Olson *et al.*, 1976), normal mode analysis (Nakamura & Doi, 1994) and conformational energy calculations (Prabhakaran *et al.*, 1985).

Among interesting features observed in the present analysis, with important implications relevant to function, we mention:

(i) A number of nucleotides in the D and T stems play a crucial role in monitoring the concerted motion of tRNA, being positioned in the global hinge-bending region. In particular, the role of the D stem seems essential, as inferred from the long stretches of nucleotides (8 to 15, 20 to 22) observed to be totally rigid in the slowest mode of motion. Interestingly, the D-helix was recently pointed out by Brion and Westhof to "form the structural anchor of tRNA L-shaped architecture", several tertiary triple interactions occurring in its deep groove (Brion & Westhof, 1997).

(ii) The results presented here for tRNA^{Phe} hold closely as for tRNA^{Asp}. Inasmuch as no specific properties related to the chemical identity of the nucleotides was considered, but only the positions of the phosphorus atoms, the results should hold for all tRNAs of class I having roughly the same backbone structure. Nucleotides in the variable loop also participate in monitoring the hinge-bending motion. This reminds us of the recent remarkable observation that only one nucleotide insertion in the variable loop of tRNA^{Leu} confers efficient serine accepting activity on the molecule (Himeno *et al.*, 1997). In fact, it might be worthwhile repeating GNM calculations for these

class II tRNAs, and exploring the effect of the length of the variable loop on the global dynamics.

(iii) Most invariant nucleotides are shown to be located at critical loci, either from stability or from functional points of view. They are almost rigid in the global mode of motion, as illustrated in Figure 3. The important role of conserved residues for the conformation of the T-loop has been emphasized by Giegé and collaborators (Romby *et al.*, 1987). The stacking of the T-loop nucleotide 59 on domain 1 was pointed out to be an essential feature of the three-dimensional form of tRNA by Cedergren and collaborators (Steinberg *et al.*, 1997). Nucleotide 59 was distinguished in the present analysis as well by its highly restricted mobility (Figure 3). The only other deeper minima in the curve were those attributed to the hinge-bending mechanism.

Dynamics of tRNA^{Gln} and GlnRS in complexed form

tRNA exhibits a drastic change in dynamic characteristics upon its complexation with the cognate synthetase as is evident from a comparison of Figures 1 and 7. The agreement between GNM predictions and experimental data is generally improved as the size of the investigated molecule, or complex, increases. This feature, also observed in our previous analyses (Bahar *et al.*, 1997, 1998a), is a direct consequence of the Central Limit Theorem stating that Gaussian distributions become exact in MULTIVARIATE SYSTEMS as the number of coupled variables approaches infinity.

The dominant (slowest) few modes of GlnRS, illustrated in Figure 9, provide information on the amplitudes of movements of domains, subdomains, or structural motifs, during the cooperative motions of the complex. Maxima therein point out regions of enhanced mobility, a property which emerges as a prerequisite for the efficient recognition of substrates. And minima are regions severely constrained, almost fixed in the global motion; these apparently assume the role of hinges in the collective conformational fluctuations. In GlnRS, the broad peak in the slowest mode ($k = 2$) coincides with the distal β-barrel, which binds to the anticodon loop; and that emerging in the dominant two modes ($2 \leqslant k \leqslant 3$) indicates the acceptor stem recognition region. These were colored green and yellow, respectively, in Figure 10. As to the deepest minima, five stretches of residues were identified (40 to 45, 260 to 270, 306 to 314, 320 to 327 and 478 to 485) by examining the dominant two modes, which coincide with the catalytic site of the enzyme. These are proposed to play a crucial role in monitoring the cooperative motion of the enzyme, relevant to its catalytic function. That the conserved motifs His-Ile-Gly-His (residues 40 to 43) and Met-Ser-Lys (268 to 270) common to class I aminoacyl-RS, are among these residues is strongly supportive of the role attributed to these residues.

Concluding remark

The direct correlation between regions exhibiting the largest amplitude displacements in the global motion (elucidated by GNM), and those actively involved in recognition or binding was also observed in other systems, including the recognition loops of HIV-1 protease (Bahar *et al.*, 1998b), the thumb and finger domains of the p66 subunit of HIV-1 reverse transcriptase (Bahar *et al.*, unpublished), and the antigen binding loops (CDRs) of immunoglobulins. Likewise, the identification of the minima in the dominant modes' distributions with hinge-bending regions, or boundaries delimiting coherently moving domains, is a feature revealed by the modal decomposition of vibrational dynamics (Holm & Sander, 1994; Bahar *et al.*, 1998b). Following upon these successes, it would seem appropriate to extend the GNM approach to protein-DNA complexes, or even to more complex systems (quaternary structures) such as those elucidated at lower resolution by electron microscopy, given the simplicity and computational efficiency of the method, and the opportunities for gaining an understanding of function through the cooperative dynamic preferences of such systems on a global scale.

Materials and Method

Gaussian network model

In this model, the change $\Delta \mathbf{R}_{ij}$ in the mean separations between "close" or "contacting" residue pairs is assumed to be controlled by the harmonic potential:

$$V(\Delta \mathbf{R}_i, \Delta \mathbf{R}_j) = 1/2\, \gamma (\Delta \mathbf{R}_j - \Delta \mathbf{R}_i) \cdot (\Delta \mathbf{R}_j - \Delta \mathbf{R}_i)$$

$$= 1/2\, \gamma \Delta \mathbf{R}_{ij}^2 \qquad (1)$$

Here $\Delta \mathbf{R}_i$ is the change in the position of residue i, $\Delta \mathbf{R}_{ij}$ is the magnitude of the vector $\Delta \mathbf{R}_j - \Delta \mathbf{R}_j$, γ is the force constant, and the symbol $\cdot$ denotes the scalar product. Correlations between residue fluctuations, $\langle \Delta \mathbf{R}_i \cdot \Delta \mathbf{R}_j \rangle$, are evaluated from the partial inverse Γ^{-1} of the Kirchhoff or adjacency matrix Γ characteristic of the investigated structure, using:

$$\langle \Delta \mathbf{R}_i \cdot \Delta \mathbf{R}_j \rangle = (3kT/\gamma)[\Gamma^{-1}]_{ij} \qquad (2)$$

where k is the Boltzmann constant and T is the absolute temperature (Flory, 1976; Pearson, 1977; Kloczkowski *et al.*, 1989; Bahar & Jernigan, 1997). The mean-square fluctuations $\langle (\Delta \mathbf{R}_i)^2 \rangle$ are thus simply given by the diagonal elements $[\Gamma^{-1}]_{ii}$ of Γ^{-1}.

The Kirchhoff matrix Γ is related to residue contact maps. For a molecule comprising n interaction sites, this is a symmetric matrix of order n. The ijth off-diagonal element of Γ is equal to -1 if sites i and j are "in contact", and zero otherwise. Two sites are assumed to be in contact if their separation is below a suitably chosen cutoff distance r_c. The diagonal elements of Γ are found from the negative sum of all off-diagonal elements in the same row (or column), and thus represent the coordination number of each nucleotide. Constructed in this form, Γ is equivalent to transition rate matrices of multivariate stochastic processes (Schuler, 1969; Bahar, 1989),

in that it controls the time evolution of fluctuations *via* a master equation of the form $d\Delta \mathbf{R}/dt \sim \Gamma\, \Delta \mathbf{R}$. Here $\Delta \mathbf{R}$ is the vector of instantaneous changes $\{\Delta \mathbf{R}_1,\, \Delta \mathbf{R}_2,\, \ldots,\, \Delta \mathbf{R}_n\}$ in nucleotide or residue positions, and the symbol $\sim$ denotes proportionality.

Application to tRNA

In the application of the GNM to tRNA in the free form, each nucleotide is assumed to represent a single interaction site located at the phosphorus atom. In the application to enzyme-bound tRNA, a finer description of the tRNA molecules is chosen in order to match more clearly the degree of resolution of the protein model (GlnRS). In the GNM description of proteins, α-carbons, separated by virtual bonds of length 3.8 Å, approximately, are considered. Similarly, we adopted two sites per nucleotide in tRNA^{Gln}, the atoms P and O$_4'$, which are separated by a distance more comparable and consistent with that of consecutive C^α–C^α atoms.

A cutoff distance r_c of 7 Å is chosen for the effective range of inter-residue contacts in GlnRS based on the analysis of protein structures (Miyazawa & Jernigan, 1985; Bahar & Jernigan, 1997). A larger cutoff distance is required for tRNA nucleotides, inasmuch as the diameter of the *A*-form RNA double helix itself is 20 Å. The distances between the P atoms on adjacent strands forming base-pairs vary in the range $13 \leqslant \mathbf{R}_{ij} \leqslant 16$ Å, which ought to be included in the effective interaction range. Results reported for tRNA^{Phe} and tRNA^{Asp} use $r_c = 19$ Å. This distance leads to an average coordination number of 17 per nucleotide. The most densely packed nucleotides are calculated to be m^{5}C49 and C60 in the T-arm; their coordination number is 34. The anticodon nucleotide Gm34 and the acceptor tetranucleotide ACCA exhibited the lowest coordination number 5. A cutoff distance of $r_c = 16$ Å is adopted for the intramolecular and intermolecular contacts of tRNA^{Gln} sites in the complex.

In the application of the GNM to uncomplexed tRNA a Kirchhoff matrix Γ of order $n = 76$ is inverted. In the case of the enzyme-bound tRNA, the size of the Kirchhoff matrix to be inverted is $(75 \times 2) + 529 = 679$, i.e. two sites per nucleotide (the coordinates of nucleotide 1 of tRNA^{Gln} were not reported; Rould *et al.*, 1991), and one site per each of the GlnRS residues (8 to 442, 454 to 547) whose X-ray coordinates are available. The inversion of the Γ matrix of this size, which is computationally the most time-consuming part of the calculation, requires less than five minutes CPU time on a R8000 Silicon Graphics Workstation.

Decomposition of conformational dynamics into a collection of modes

The vibrational dynamics of a macromolecular system results from the superposition of several modes of motion. In the GNM, it is possible to extract the contribution of the kth mode ($2 \leqslant k \leqslant n$) by an eigenvalue decomposition of Γ (Haliloglu *et al.*, 1997). This yields a total of $n - 1$ modes, the frequencies of which are equal to the non-zero eigenvalues λ_k of Γ. The eigenvalues are usually organized in ascending order, i.e. $\lambda_1 = 0 < \lambda_2 \leqslant \lambda_3 \leqslant \ldots \leqslant \lambda_n$. The slowest mode, which is generally of interest for extracting information on the global motions, is therefore assigned the index 2. The cross-correlation $\langle \Delta \mathbf{R}_i \cdot \Delta \mathbf{R}_j \rangle_k$ contributed by the kth

mode is found from the kth eigenvector $\mathbf{u}_k$ of Γ as:

$$\langle \Delta \mathbf{R}_i \cdot \Delta \mathbf{R}_j \rangle_k = (3kT/\gamma)[\lambda_k^{-1} \mathbf{u}_k \mathbf{u}_k^T]_{ij} \equiv (3k_B T/\gamma)\lambda_k^{-1} u_{ij}^{(k)} \quad (3)$$

Here $u_{ij}^{(k)}$ denotes the ijth element of the matrix $[\mathbf{u}_k \mathbf{u}_k^T]$. We note that (i) the proportionality constant $(3kT/\gamma)$ is eliminated when the orientational cross-correlations:

$$C_{ij} \equiv \langle \Delta \mathbf{R}_i \cdot \Delta \mathbf{R}_j \rangle / [\langle \Delta \mathbf{R}_i \cdot \Delta \mathbf{R}_i \rangle \langle \Delta \mathbf{R}_j \cdot \Delta \mathbf{R}_j \rangle]^{1/2} \quad (4)$$

are examined, and (ii) the factor λ_k^{-1} plays the role of a statistical weight, which suitably rescales the contributions of the individual modes. For example, the correlations conveyed by the several modes $k_1 \leqslant k \leqslant k_2$ of interest are given by:

$$C_{ij}(k_1 \leqslant k \leqslant k_2) \equiv \Sigma_k \lambda_k^{-1} u_{ij}^{(k)} / [\Sigma_k \lambda_k^{-1} u_{ii}^{(k)} \Sigma_k \lambda_k^{-1} u_{jj}^{(k)}]^{1/2} \quad (5)$$

where the summations are only over the investigated modes $k_1 \leqslant k \leqslant k_2$.

Acknowledgement

References

Abola, E. E., Bernstein, F. C., Bryant, S. H., Koetzle, T. F. & Weng, J. (1987). In *Crystallographic Databases–Information Content Software Systems, Scientific Applications* (Allen, F. H., Bergerhoff, G. & Sievers, R., eds), p. 107, Data Commission of the International Union of Crystallography, Bonn, Cambridge and Chester.

Bahar, I. (1989). Stochastics of rotational isomeric transitions in polymer chains. *J. Chem. Phys.* **91**, 6525–6531.

Bahar, I. & Jernigan, R. L. (1997). Inter-residue potentials in globular proteins and the dominance of highly specific hydrophilic interactions at close separation. *J. Mol. Biol.* **266**, 195–214.

Bahar, I., Atilgan, A. R. & Erman, B. (1997). Direct evaluation of thermal fluctuations in proteins using a single parameter harmonic potential. *Folding Design,* **2**, 173–181.

Bahar, I., Wallqvist, A., Covell, D. & Jernigan, R. L. (1998a). Correlation between hydrogen exchange from native proteins and cooperative residue fluctuations from a simple model. *Biochemistry,* **37**, 1067–1075.

Bahar, I., Atilgan, A. R., Demirel, M. C. & Erman, B. (1998b). Vibrational dynamics of folded proteins: Significance of slow and fast modes in relation to function and stability. *Phys. Rev. Letters,* **80**, 2733–2736.

Bernstein, F. C., Koetzle, T. F., Williams, G. J. B., Meyer, E. F. J., Brice, M. D., Rodgers, J. R., Kennard, O., Shimanouchi, T. & Tasumi, M. (1977). The Protein data bank: A computer-based archival file for macromolecular structures. *J. Mol. Biol.* **112**, 535–542.

Brion, P. & Westhof, E. (1997). Hierarchy and dynamics of RNA folding. *Annu. Rev. Biophys. Biomol. Struct.* **26**, 113–137.

Flory, P. J. (1976). Statistical thermodynamics of random networks. *Proc. Roy. Soc. London, ser. A,* **351**, 351–380.

Frauenfelder, H., Petsko, A. & Tsernoglou, D. (1979). Temperature dependent X-ray diffraction as a probe of protein structural dynamics. *Nature,* **280**, 558–563.

Gu, X., Ivanetich, K. & Santi, D. V. (1996). Recognition of the T-arm of tRNA by tRNA (M5U54)-methyltransferase is not sequence specific. *Biochemistry,* **35**, 11652–11659.

Haliloglu, T., Bahar, I. & Erman, B. (1997). Gaussian dynamics of folded proteins. *Phys. Rev. Letters,* **79**, 3090–3093.

Harvey, S. C. & Gabb, H. A. (1993). Conformational transitions using molecular dynamics with minimum biasing. *Biopolymers,* **33**, 1167–1172.

Harvey, S. C., Prabhakaran, M. & McCammon, J. A. (1985). Molecular dynamics simulations of phenylalanine tRNA. I. Methods and general results. *Biopolymers,* **24**, 1169–1188.

Himeno, H., Yoshida, S., Soma, A. & Nishikawa, K. (1997). Only one nucleotide insertion to the long variable arm confers an efficient serine acceptor activity upon *Saccharomyces cerevisiae* tRNA$^{\text{Leu}}$ in vitro. *J. Mol. Biol.* **268**, 704–711.

Hingerty, B., Brown, R. S. & Jack, A. (1978). Further refinement of the structure of yeast tRNA$^{\text{Phe}}$. *J. Mol. Biol.* **124**, 523–534.

Holm, L. & Sander, C. (1994). Parser for protein folding units. *Proteins: Struct. Funct. Genet.* **19**, 256–268.

Jack, A., Ladner, J. E. & Klug, A. (1976). Crystallographic refinement of yeast phenylalanine transfer RNA at 2.5 resolution. *J. Mol. Biol.* **108**, 619–649.

Jernigan, R. L. & Bahar, I. (1998). Conformational search: proteins. In *Encyclopedia of Computational Chem.* in the press.

Kloczkowski, A., Mark, J. E. & Erman, B. (1989). Chain dimensions and fluctuations in random elastomeric networks. 1. Phantom Gaussian networks in the undeformed state. *Macromolecules,* **22**, 1423–1432.

McCammon, J. A. & Harvey, S. C. (1987). *Dynamics of Proteins and Nucleic Acids*, Cambridge University Press.

Miyazawa, S. & Jernigan, R. L. (1985). Estimation of effective interresidue contact energies from protein crystal structures: quasi-chemical approximation. *Macromolecules,* **18**, 534–552.

Nakamura, S. & Doi, J. (1994). Dynamics of transfer RNAs analyzed by normal mode calculations. *Nucl. Acids Res.* **22**, 514–522.

Olson, T., Fournier, M. J., Langley, K. H. & Ford, N. C., Jr (1976). Detection of a major conformational change in transfer ribonucleic acid by laser light scattering. *J. Mol. Biol.* **102**, 193–203.

Pearson, D. S. (1977). Scattered intensity from a chain in a rubber network. *Macromolecules,* **10**, 696–701.

Perona, J. J., Rould, M. A. & Steitz, T. A. (1993). Structural basis for transfer RNA aminoacylation by *Escherichia coli* glutaminyl-tRNA synthetase. *Biochemistry,* **32**, 8758–8771.

Prabhakaran, M., Harvey, S. C. & McCammon, J. A. (1985). Molecular-dynamics simulation of phenylalanine transfer RNA. II. Amplitudes, anisotropies, and anharmonicities of atomic motions. *Biopolymers,* **24**, 1189–1204.

Rigler, R. & Wintermeyer, W. (1983). Dynamics of tRNA. *Annu. Rev. Biophys. Bioeng.* **12**, 475–505.

Robertus, J. D., Ladner, J. E., Finch, J. T., Rhodes, D., Brown, R. S., Clark, B. F. C. & Klug, A. (1974). Structure of yeast phenylalanine tRNA at 3 Å resolution. *Nature,* **250,** 546–551.

Romby, P., Carbon, P., Westhof, E., Ehresmann, C., Ebel, J., Ehresmann, B. & Giegé, R. (1987). Importance of conserved residues for the conformation of the T-loop in tRNAs. *J. Biomol. Struct. Dynam.* **5,** 669–687.

Rould, M. A., Perona, J. J., Dieter, S. & Steitz, T. A. (1989). Structure of *E. coli* glutaminyl-tRNA synthetase complexed with tRNA^{Gln} and ATP at 2. 8 Å resolution. *Science,* **246,** 1135–1142.

Rould, M. A., Perona, J. J. & Steitz, T. A. (1991). Structural basis of anticodon loop recognition by glutaminyl-tRNA synthetase. *Nature,* **352,** 213–218.

Schimmel, P. & dePoupiana, L. R. (1995). Transfer RNA: from minihelix to genetic code. *Cell,* **81,** 983–986.

Schuler, K. E., ed. (1969). *Stochastic Processes in Chemical Physics.* In *Advan. Chem. Phys.,* Interscience Publ., New York.

Steinberg, S., Leclerc, F. & Cedergren, R. (1997). Structural rules and conformational compensations in the tRNA L-form. *J. Mol. Biol.* **266,** 269–282.

Sussman, J. L., Holbrook, S. R., Warrant, R. W., Church, G. M. & Kim, S. (1978). Crystal structure of yeast phenylalanine tRNA. I. Crystallographic refinement. *J. Mol. Biol.* **123,** 607–630.

Tirion, M. M. (1996). Large amplitude elastic motions in proteins from a single-parameter atomic analysis. *Phys. Rev. Letters,* **77,** 1905–1908.

Tung, C. S., Harvey, S. C. & McCammon, J. A. (1984). Large-amplitude bending motions in phenyl alanine transfer RNA. *Biopolymers,* **23,** 2173–2193.

Westhof, E. & Sundaralingam, M. (1986). Restrained refinement of the monoclinic form of yeast phenylalanine transfer RNA. Temperature factors and dynamics, coordinated waters, and base-pair propeller twist angles. *Biochemistry,* **25,** 4868–4878.

Westhof, E., Dumas, P. & Moras, D. (1988). Restrained refinement of two crystalline forms of yeast aspartic acid and phenylalanine transfer RNA crystals. *Acta Crystallog. sect. A,* **A44,** 112–123.

Edited by I. Tinoco